

Biomimetic coating of an apatite layer on poly(L-lactic acid); improvement of adhesive strength of the coating

Yoshiro Yokoyama · Ayako Oyane · Atsuo Ito

Received: 1 September 2005 / Accepted: 5 May 2006 / Published online: 5 May 2007
© Springer Science+Business Media, LLC 2007

Abstract A biodegradable polymer coated with a bone-like apatite layer on its surface would be useful as a scaffold for bone tissue regeneration. In this study, poly(L-lactic acid) (PLLA) was treated with oxygen plasma to produce oxygen-containing functional groups on its surface. The plasma-treated specimen was then alternately dipped in aqueous CaCl_2 and $\text{K}_2\text{HPO}_4 \cdot 3\text{H}_2\text{O}$ solutions three times, to deposit apatite precursors onto the surface. The surface-modified specimen then successfully formed a dense and uniform bonelike surface apatite layer after immersion for 24 h in a simulated body fluid with ion concentrations approximately equal to those of human blood plasma. The adhesive strength between the apatite layer and the specimen surface increased as the power density of the oxygen plasma used increased. The maximum adhesive strength of the apatite layer to the specimen was significantly higher than that to the commercially available artificial bone, HAPEXTM. The resultant bonelike apatite–PLLA composite would be useful as a scaffold for bone tissue regeneration.

Introduction

Tissue engineering has recently emerged as a promising approach for bone repair and reconstruction [1, 2]. In this approach, patient-derived bone cells are implanted onto a scaffold to initiate the generation of new natural bone tissues. A biodegradable scaffold serves as a physical support to guide new tissue growth, before degrading and eventually being replaced by the new tissues.

A biodegradable polymer coated with a bonelike apatite layer on its surface is likely to be highly appropriate as a scaffold for bone tissue regeneration [3], since apatite is a major inorganic component of natural bone, and exhibits good biocompatibility and osteoconductivity [4, 5]. Over the past decade, various coating techniques, including biomimetic [6–13], alternate soaking [14, 15], spray coating [16], laser deposition [17], coupling [18], and low-temperature precipitation [19] processes have been developed to deposit apatite on the surfaces of polymeric materials. Among these coating techniques, the biomimetic process [6–13] is intrinsically suitable for production of bonelike apatite on polymer surfaces. In this process, the polymer surface is modified with functional groups that are effective in inducing apatite nucleation, and is then immersed in a simulated body fluid (SBF) [20] having ion concentrations approximately equal to those of human blood plasma. Although Si–OH [6, 7], Ti–OH [8], –COOH [9, 10], – PO_4H_2 [11] and – SO_3H [12, 13] have been the functional groups tested, the apatite-forming ability of these functional groups is so weak that they require a long period to induce apatite formation in an SBF. Therefore, they may need to be combined with calcium ions [6, 7, 9–13] or arranged in a certain structure [8, 21] to accelerate apatite nucleation in SBF.

We have recently succeeded in markedly reducing the induction period for apatite formation on poly(ϵ -caprolactone)

Y. Yokoyama · A. Oyane (✉)
Nanotechnology Research Institute, National Institute of
Advanced Industrial Science and Technology (AIST), Central 4,
1-1-1, Higashi, Tsukuba-shi, Ibaraki 305-8562, Japan
e-mail: a-oyane@aist.go.jp

A. Ito
Institute for Human Science and Biomedical Engineering,
National Institute of Advanced Industrial Science and
Technology (AIST), Central 6, 1-1-1, Higashi, Tsukuba-shi,
Ibaraki 305-8566, Japan

(PCL) in SBF, by applying a simple surface modification process to PCL [22]. In this modification process, PCL was treated with oxygen plasma to produce oxygen-containing functional groups on its surface, and it was then subsequently dipped alternately in calcium ion and phosphate ion solutions to deposit apatite precursors onto the surface. The surface-modified PCL successfully formed a dense and uniform bonelike apatite layer on its surface after only 24 h immersion in SBF.

Poly(L-lactic acid) (PLLA) is superior in mechanical properties to PCL. Although PCL is biodegradable, biocompatible, and can be easily molded owing to its low melting point [23], it is limited in applicability because of its low tensile strength and Young's modulus. In contrast, PLLA has been widely used in clinical applications, including bone fixation materials and scaffolds for tissue engineering, because of its high tensile strength and Young's modulus [3, 24, 25]. Therefore, from a practical point of view, it would be beneficial if the above-mentioned surface modification process used for PCL could also be successfully applied to PLLA to produce a bonelike apatite-PLLA composite.

In this study, PLLA was subjected to the same surface modification process used for PCL, namely, oxygen plasma treatment followed by alternate dipping in calcium ion and phosphate ion solutions. The apatite-forming ability of the surface-modified specimens was examined in SBF. The adhesive strength of the apatite layer, which was formed in SBF, to the specimen was also investigated, and compared with that to a commercially available artificial bone, HAPEX™ [26]. The results are discussed in terms of the surface structural changes of PLLA due to the surface modification process and subsequent immersion in SBF.

Experimental

Preparation of specimens

A PLLA plate, 1 mm in thickness, was prepared by hot-pressing PLLA pellets (Shimazu Co., Japan, Average Mn = 200,000 (GPC)) at 265 °C. The PLLA plate was cut into square pieces, 10 × 10 mm² in size. The specimens were ultrasonically washed with ethanol for 30 min, and dried under vacuum at 50 °C for 24 h.

Plasma treatment

The PLLA specimens were subjected to oxygen plasma treatment. The plasma treatment was carried out in O₂ gas (99.999%) at a pressure of 30 Pa under an electric field operating at 13.56 MHz for 30 s, using a compact ion etcher (FA-1, SAMCO Inter. Inc., Japan). The plasma power density was varied from 0.10 to 1.00 W/cm².

Alternate dipping in calcium ion and phosphate ion solutions

The untreated and plasma-treated specimens were dipped alternately in calcium ion and phosphate ion solutions using the following process [14, 15, 22]. A specimen was hung on a platinum wire having a diameter of 0.5 mm. Using the wire, the specimen was dipped in 20 mL of 200 mM CaCl₂ (Nacalai Tesque Inc., Japan) for 10 s, dipped in 20 mL of ultra-pure water for 1 s and then dried in air for a few minutes. The specimen was subsequently dipped in 20 mL of 200 mM K₂HPO₄·3H₂O (Nacalai Tesque Inc., Japan) for 10 s, dipped in 20 mL of ultra-pure water for 1 s and then dried in air for a few minutes. The dipping and lifting rate was fixed at 50 cm/min using a linear head motor equipped with a speed controller (Oriental Motor Co., Ltd, Japan). The above procedure of alternate dipping in calcium ion and phosphate ion solutions was performed three times at room temperature. The same CaCl₂ and K₂HPO₄·3H₂O solutions and ultra-pure water were used for a given specimen throughout the three cycles of alternate dipping.

Immersion in SBF

The surface-modified specimens and HAPEX [26] as a control were immersed in 30 mL of an SBF [20] with ion concentrations (Na⁺ 142.0 mM, K⁺ 5.0 mM, Mg²⁺ 1.5 mM, Ca²⁺ 2.5 mM, Cl⁻ 147.8 mM, HCO₃⁻ 4.2 mM, HPO₄²⁻ 1.0 mM, SO₄²⁻ 0.5 mM) approximating those present in human blood plasma, at 36.5 °C. The apatite-forming ability of the surface-modified specimens was assessed after 24 h immersion in SBF. However, measurements of the adhesive strength of the apatite layer, formed in SBF, and the specimen were made after immersion for 8 d, with the spent SBF replaced with a fresh fluid after 4 d immersion. The SBF was prepared by dissolving NaCl, NaHCO₃, KCl, K₂HPO₄·3H₂O, MgCl₂·6H₂O, CaCl₂, and Na₂SO₄ (Nacalai Tesque Inc., Japan) in ultra-pure water and buffering the solution at pH 7.40 at 36.5 °C with tris(hydroxymethyl)aminomethane (final concentration of 50 mM) and 1 M HCl (Nacalai Tesque Inc, Japan) [27]. After removal from the SBF, the specimen was gently washed with ultra-pure water and then dried in air at room temperature.

Surface characterization

The surface structures of the specimens were examined using an X-ray photoelectron spectrometer (XPS; Quantum-2000, ULVAC-PHI Inc., Japan) with Al K α X-rays, a thin-film X-ray diffractometer (TF-XRD; Rint 2500VH/PC, Rigaku Co., Japan) with Cu K α X-rays, and a scanning

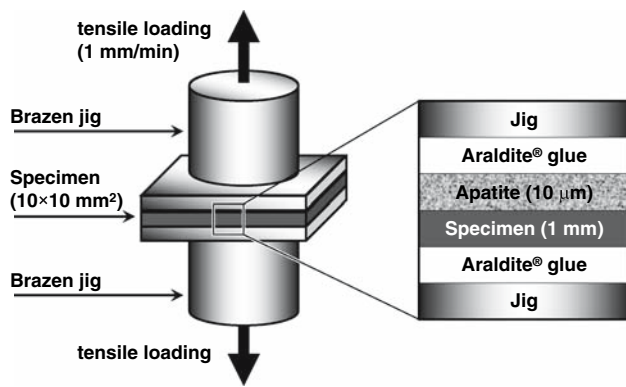


Fig. 1 Arrangement for measuring adhesive strength between the apatite layer and the specimen

electron microscope (SEM; XL30, FEI Company Japan Ltd., Japan). The photoelectron take-off angle was set at 45° for XPS. Binding energies measured by XPS were corrected by defining the binding energy of the C_{1s} in the CH_2 group as 284.6 eV. For TF-XRD, the glancing angle of the specimen was set at 1° against the direction of the incident beam.

Measurement of adhesive strength

The adhesive strength of the apatite layer to the specimen was measured under tensile stress [28]. Both sides of the specimen, on only one side of which the $10\ \mu\text{m}$ -thick apatite layer was formed, were attached to brazen jigs with a base of $10 \times 10\ \text{mm}^2$ using Rapid-type Araldite[®] glue (Vantico K. K., Japan), as shown in Fig. 1. The specimen was subsequently left untouched overnight for complete solidification of the glue. Tensile load was applied to the specimen using an Instron-type testing machine (UCT-500, Orientec Co., Japan) at a crosshead speed of 1 mm/min until fracture occurred. Eight plates were tested for each type of specimen, to allow calculation of the means and standard deviations of the adhesive strength. The data were assessed using a one-way ANOVA followed by the Fisher's protected least significant difference test. Differences at $p < 0.05$ were considered to be statistically significant. Structures on the fractured surfaces were examined using SEM equipped with an energy dispersive electron probe X-ray analyzer (EDX; Genesis 2000, EDAX Japan K. K., Japan).

Results

Surface structural changes of the specimen due to plasma treatment

Figure 2a shows C_{1s} XPS spectra of surfaces of untreated and plasma-treated PLLA specimens. The original C_{1s} peak

(solid line) was resolved into five components (dotted line) with binding energies of 284.6, 286.5, 287.6, 288.7, and 290.3 eV, which were attributed to carbon atoms in $-C-C-$, $-C-O-$, $-C=O$ or $-O-C-O-$, $-O-C=O$, and $-O-C(=O)-O-$, respectively [29, 30]. The intensities of the latter four peaks increased after the plasma treatment. In contrast, the intensity of the former single peak decreased after the plasma treatment. From these results, we consider that the methylene and ester linkages on the specimen surface were partially cleaved by the plasma treatment to produce oxygen-containing functional groups such as hydroxyl, carbonyl, and carboxyl groups. This hypothesis was further confirmed by surface compositional analysis of these specimens, as shown in Fig. 2b. The surface atomic concentrations of C and O on the specimens were calculated from the peak area of each atom in the XPS spectra. As shown in the figure, the surface concentration of C decreased with increasing plasma power density, whereas that of O increased. This result indicates that the oxygen-containing functional groups on the surface of the plasma-treated specimens increased in density with increasing plasma power density.

Figure 3 shows SEM photographs of the surfaces of an untreated PLLA specimen and specimens treated with oxygen plasma at power densities of 0.10, 0.50, 0.75, and $1.00\ \text{W}/\text{cm}^2$. The untreated specimen and specimens treated with oxygen plasma at power densities of 0.10 and $0.50\ \text{W}/\text{cm}^2$ had flat and smooth surfaces at the nano-scale. In contrast, specimens treated with plasma at power densities of 0.75 and $1.00\ \text{W}/\text{cm}^2$ had surfaces with a large number of nano-sized granules. The size of the granules on a specimen increased with increasing plasma power density. These granules are considered to be formed via cleavage of methylene and ester linkages at the specimen surface, and subsequent etching of the degraded portion during plasma treatment [31]. It was found from these results that the surface roughness of the plasma-treated specimens increased with increasing plasma power density.

Surface structural changes of the specimen due to alternate dipping treatment

The surface structures of the specimen subjected to alternate dipping treatment without plasma treatment (P000), and the specimens treated with oxygen plasma at power densities of 0.10 (P010), 0.50 (P050), 0.75 (P075), and $1.00\ \text{W}/\text{cm}^2$ before being subjected to alternate dipping treatment, were examined by XPS. Peaks due to Ca and P were readily detected only for P050, P075, and P100, whereas they were hardly detected for P000 and P010. Atomic ratios of Ca/C and P/C were calculated from the peak area of each atom in the XPS spectra, and the results

Fig. 2 C_{1s} XPS spectra of surfaces of untreated and plasma-treated PLLA (a), and surface atomic concentrations of C and O (b)

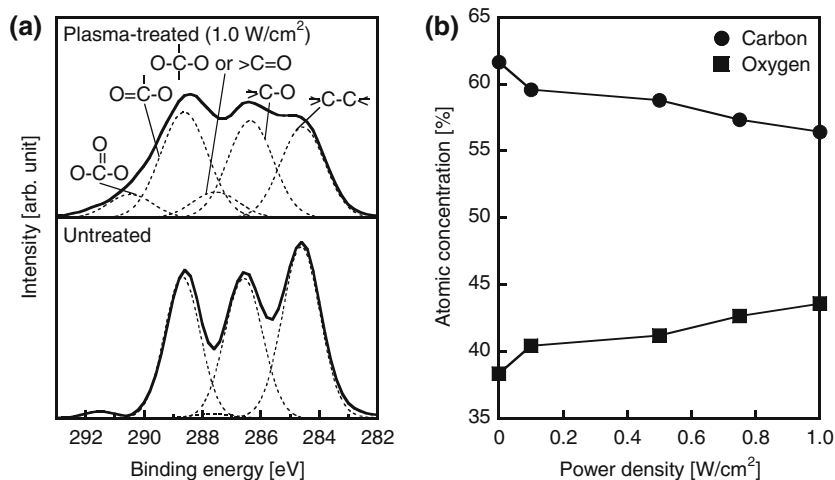
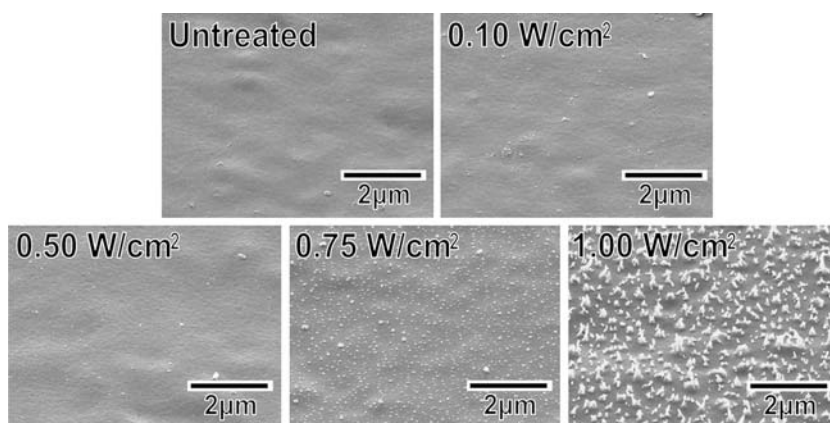


Fig. 3 SEM photographs of surfaces of untreated PLLA, and specimens treated with oxygen plasma at power densities of 0.10, 0.50, 0.75, and 1.00 W/cm²



are shown in Fig. 4. It can be seen from the figure that a certain type of calcium phosphate was deposited onto the surfaces of P050, P075, and P100, but not onto the surfaces of P000 and P010. TF-XRD measurements were also performed on these specimens. However, no peaks ascribed to apatite were detected. Taking into account the results of a previous report [32], the calcium phosphate deposited onto the surfaces of P050, P075, and P100 is likely to be amorphous calcium phosphate (ACP).

Figure 5 shows SEM photographs of the surfaces of P000, P010, P050, P075, and P100. The surface morphologies of P000 and P010 were almost identical to those observed before alternate dipping treatment (see Fig. 3). In the case of P050, new nano-sized granules were observed after alternate dipping treatment. In the cases of P075 and P100, nano-sized granules, which were observed on the plasma-treated specimens, increased in size after alternate dipping treatment. The morphological differences observed in P050, P075, and P100 before and after alternate dipping treatment are attributed to the deposition of calcium phosphate onto the specimen surface as a result

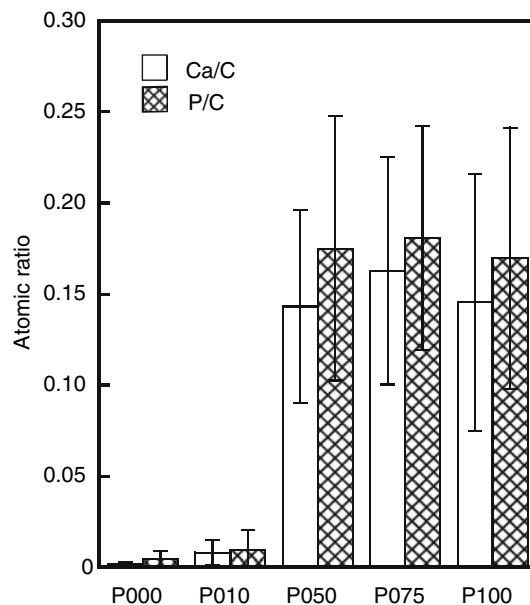
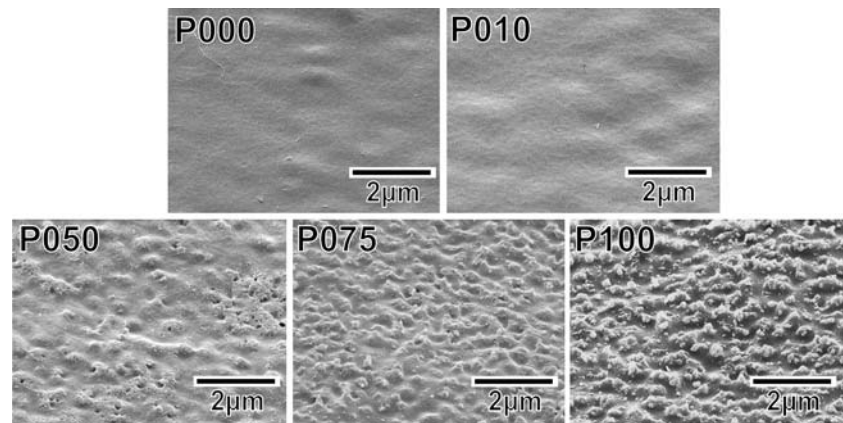


Fig. 4 Atomic ratios of Ca/C and P/C at surfaces of P000, P010, P050, P075, and P100

Fig. 5 SEM photographs of surfaces of P000, P010, P050, P075, and P100



of the treatment, according to the XPS results shown in Fig. 4.

Apatite-forming ability of surface-modified specimens in SBF

Peaks ascribable to apatite [33] were observed in the TF-XRD patterns of the surfaces of P050, P075, and P100 after immersion in SBF for 24 h, as shown in Fig. 6. For P000 and P010, no peaks ascribable to apatite were observed after immersion in SBF. Figure 7 shows SEM photographs of the surfaces of these specimens. The surface structures of P000 and P010 after immersion in SBF

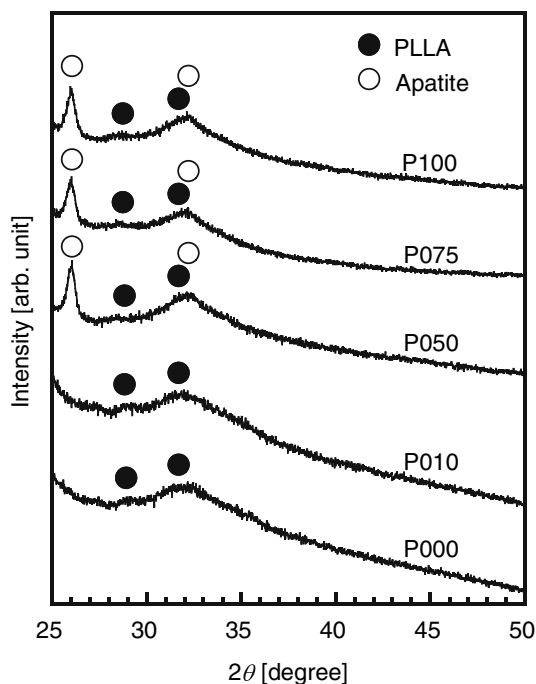


Fig. 6 TF-XRD patterns of surfaces of P000, P010, P050, P075, and P100, after immersion in SBF for 24 h

were almost the same as those seen before immersion (see Fig. 5). In contrast, a layer with a nano-porous structure was observed over the entire surfaces of P050, P075, and P100 after immersion in SBF. According to the XRD data shown in Fig. 6, this layer is likely to be composed of apatite.

Adhesive strength of the apatite layer

As a result of immersion in SBF for 8 d, a dense and uniform apatite layer with a thickness of about 10 μm was formed on the surfaces of P050, P075, P100, and HAPEX. Figure 8 shows the adhesive strengths of the apatite layers measured for these specimens. It can be seen from Fig. 8 that the adhesive strength improved in the order: P050 (1.94 ± 0.42 MPa) < P075 (2.60 ± 0.69 MPa) < HAPEX (4.68 ± 0.40 MPa) < P100 (6.40 ± 1.12 MPa). The adhesive strength of the apatite layer to P100 was significantly higher than to HAPEX.

SEM photographs of the fractured surfaces of the specimen side and the corresponding jig side, and schematic presentations of the failure modes are shown in Fig. 9. In the cases of P050 and P075, dense and smooth surfaces were observed on both the jig and the specimen sides. On the jig side, Ca and P, which are component elements of apatite, were detected by EDX, whereas they were not detected on the specimen side (not shown). This indicates that the fracture occurred at the apatite-specimen interface, as shown in the schematic presentations of the failure modes of P050 and P075. In the case of P100, a splintered layer with a micro-scale thickness was observed on both the jig and the specimen sides. Ca and P were detected by EDX (not shown) in this layer, indicating that it was composed of apatite. These results suggest that the fracture occurred both at the apatite–glue interface and the apatite–specimen interface, as shown in the schematic presentation of the failure mode of P100.

Fig. 7 SEM photographs at different magnifications of surfaces of P000, P010, P050, P075, and P100, after immersion in SBF for 24 h

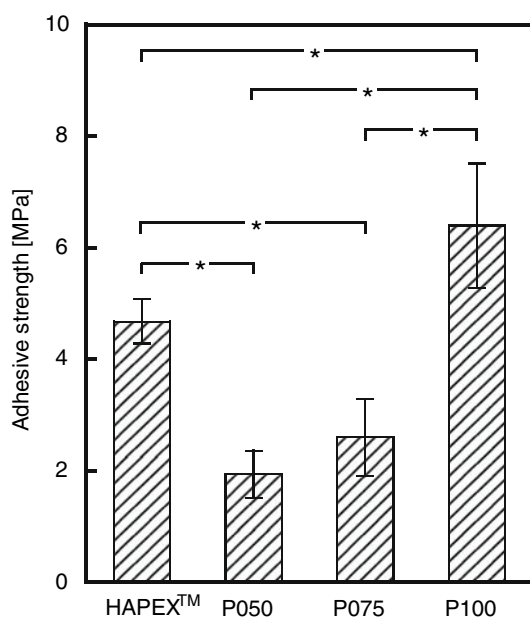
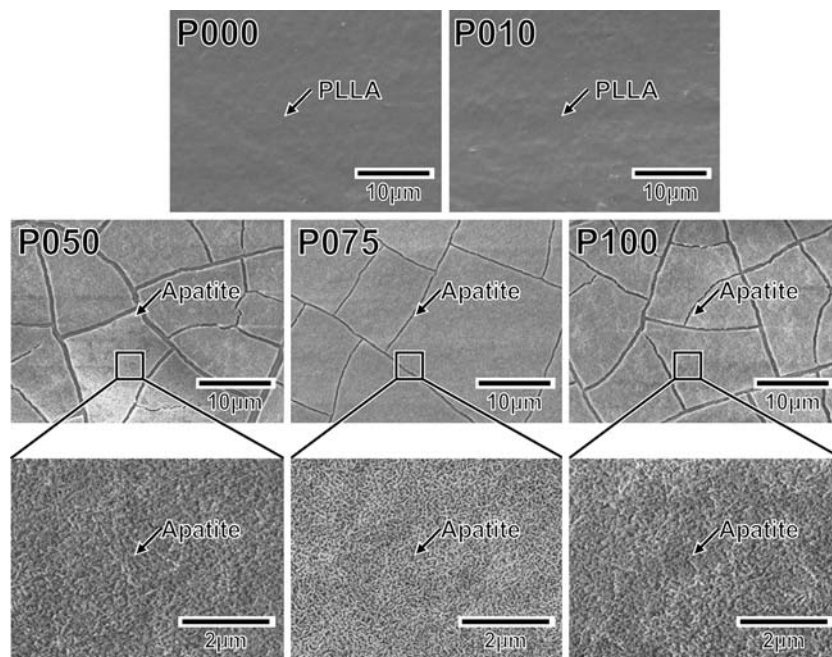


Fig. 8 Adhesive strengths of the apatite layer to surfaces of P050, P075, P100, and HAPEX as a control ($n = 8$, *: $p < 0.05$)

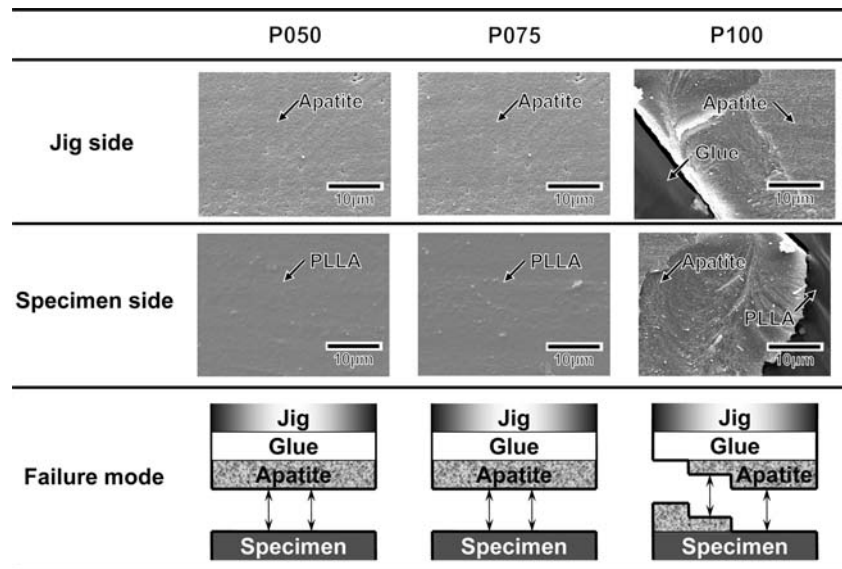
Discussion

An apatite-forming ability of PLLA in SBF was induced using the present surface modification process, i.e., plasma treatment followed by alternate calcium and phosphate ion dipping treatments. The apatite-forming ability of PLLA is considered to be induced as a result of the calcium phosphate deposited onto the surface-modified specimen. As shown in Figs. 6 and 7, apatite-forming ability was induced

only for P050, P075, and P100 with calcium phosphate deposition, but not for P000 and P010 without calcium phosphate deposition. The calcium phosphate deposited on P050, P075, and P100 is likely to be ACP, based on our XRD results and our previous report [32]. The ACP on the specimens grew and induced nucleation of apatite and/or octacalcium phosphate on the PLLA surface in SBF. This is because the SBF is supersaturated with respect to apatite and octacalcium phosphate, and saturated or slightly supersaturated with respect to ACP (based on calculations using the method described in References 34 and 35). The ACP and/or octacalcium phosphate eventually transformed into apatite, since apatite has the lowest solubility and is the most stable phase among all the calcium phosphates in aqueous solution at neutral pH [36]. Once the apatite formed, it grew spontaneously by consuming either calcium and phosphate ions, or calcium phosphate clusters [34, 35] from the surrounding SBF.

An essential requirement for the deposition of calcium phosphate (ACP) onto a specimen surface by alternate dipping treatment is likely to be the presence of surface functional groups at a certain density [22]. The functional groups on the specimen surface decrease interfacial tension between the surface and the solutions used in the alternate dipping treatment [22]. When a plasma-treated specimen is first dipped in the calcium solution, the surface functional groups attract positively charged calcium ions from the solution. When the specimen is subsequently dipped in the phosphate ion solution, calcium ions on the specimen surface attract negatively charged phosphate ions from the solution. As a result of the alternate dipping procedure,

Fig. 9 SEM photographs of the fractured surfaces of the specimens P050, P075, and P100 (specimen side), and the corresponding jigs (jig side), and schematic presentations of the failure modes at the interface between the apatite layer and the specimen



calcium phosphate is deposited onto the specimen surface via the electrostatic interaction between the functional groups, and calcium and phosphate ions in the solutions used in the alternate dipping treatment. Owing to the important role of the surface functional groups, calcium phosphate was deposited on the surfaces of P050, P075, and P100, but not on the surfaces of P000 and P010 (Figs. 4 and 5).

The adhesive strength between the apatite layer and the specimen surface improved with increasing power density in the plasma treatment ($P050 < P075 < P100$). The increase in plasma power density caused an increase in both the density of functional groups (Fig. 2) and the roughness (Fig. 3) on the specimen surface. The increase in density of the surface functional groups improved adhesive strength at the apatite–specimen interface because of an electrostatic anchoring effect between the apatite layer and the functional groups. The increase in surface roughness improved adhesive strength at the apatite–specimen interface due to a mechanical interlocking effect. It should be noted that the adhesive strength of the apatite layer to the P100 surface was significantly higher than that to the commercially available artificial bone, HAPEX. The key technique in this surface modification process is oxygen plasma treatment, which is performed within a short period with little impact on the intrinsic physical and chemical properties of the bulk polymer. This surface modification process is, therefore, effective in producing bonelike apatite–polymer composites useful as scaffolds for bone tissue regeneration.

Conclusion

A bonelike apatite layer was successfully formed on the surface of PLLA in SBF within 24 h, when the PLLA was

previously treated with oxygen plasma and then dipped alternately in calcium ion and phosphate ion solutions. The adhesive strength between the apatite layer and the specimen surface increased as the power density of the oxygen plasma treatment increased. The maximum adhesive strength of the apatite layer to the specimen was significantly higher than that to the commercially available artificial bone, HAPEX. The resultant bonelike apatite–PLLA composite could be useful as a scaffold for bone tissue regeneration.

Acknowledgements This work was supported by Industrial Technology Research Grant Program in 2003 from the New Energy and Industrial Technology Development Organization (NEDO) of Japan.

References

1. A. G. MIKOS, A. J. THORSEN, L. A. CZERWONKA, Y. BAO, R. LANGER, D. N. WINSLOW and J. P. VACANTI, *Polymer* **5** (1994) 1068
2. C. A. VACANTI and J. P. VACANTI, *Otolaryngol. Clin. North Am.* **27** (1994) 263
3. C. M. COWAN, Y. Y. SHI, O. O. AALAMI, Y. F. CHOU, C. MARI, R. THOMAS, N. QUARTO, C. H. CONTAG, B. WU and M. T. LONGAKER, *Nature Biotech.* **22** (2004) 560
4. M. JARCHO, J. F. KAY, H. P. DROBECK and R. H. DREMUS, *J. Bioeng.* **1** (1976) 79
5. R. E. HOLMES, R. W. BUCHOLZ and V. MOONEY, *J. Orthopaedic. Res.* **5** (1987) 114
6. K. HATA, T. KOKUBO, T. NAKAMURA and T. YAMAMURO, *J. Am. Ceram. Soc.* **78** (1995) 1049
7. A. OYANE, M. KAWASHITA, K. NAKANISHI, T. KOKUBO, M. MINODA, T. MIYAMOTO and T. NAKAMURA, *Biomaterials* **24** (2003) 1729
8. A. OYANE, M. KAWASHITA, T. KOKUBO, M. MINODA, T. MIYAMOTO and T. NAKAMURA, *J. Ceram. Soc. Japan* **110** (2002) 248

9. M. KAWASHITA, M. NAKAO, M. MINODA, H. M. KIM, T. BEPPU, T. MIYAMOTO, T. KOKUBO and T. NAKAMURA, *Biomaterials* **24** (2003) 2477
10. T. MIYAZAKI, C. OHTSUKI, Y. AKIOKA, M. TANIHARA, J. NAKAO, Y. SAKAGUCHI and S. KONAGAYA, *J. Mater. Sci. Mater. Med.* **14** (2003) 569
11. P. L. GRANJA, M. A. BARBOSA, L. POUYSÉGU, B. De JÉSO, F. ROUAIS and C. BAQUEY, *J. Mater. Sci.* **36** (2001) 2163
12. I. B. Leonor, H. M. Kim, F. Balas, M. Kawashita, R. L. Reis, T. Kokubo, T. Nakamura, *Key Eng. Mater.* **284–286** (2005) 453
13. T. KAWAI, C. OHTSUKI, M. KAMITAKAHARA, T. MIYAZAKI, M. TANIHARA, Y. SAKAGUCHI and S. KONAGAYA, *Biomaterials* **25** (2004) 4529
14. T. TAGUCHI, A. KISHIDA and M. AKASHI, *Chem. Lett.* **8** (1998) 711
15. T. TAGUCHI, Y. MURAOKA, H. MATSUYAMA, A. KISHIDA and M. AKASHI, *Biomaterials* **22** (2001) 53
16. Y. SHIKINAMI and H. KAWARADA, *Biomaterials* **19** (1998) 617
17. E. N. ANTONOV, V. N. BAGRATASHVILI, L. I. KROTOVA and V. K. POPOV, *Key Eng. Mater.* **192(1)** (2000) 63
18. T. FURUZONO, K. SONODA and J. TANAKA, *J. Biomed. Mater. Res.* **56** (2001) 9
19. H. M. KIM, Y. KIM, S. J. PARK, C. REY, H. M. LEE, M. J. GLIMCHER and J. S. KO, *Biomaterials* **21** (2000) 1129
20. T. KOKUBO, H. KUSHITANI, S. SAKKA, T. KITSUGI and T. YAMAMURO, *J. Biomed. Mater. Res.* **24** (1990) 723
21. A. TAKEUCHI, C. OHTSUKI, T. MIYAZAKI, M. KAMITAKAHARA, S. OGATA, M. YAMAZAKI, Y. FURUTANI, H. KINOSHITA and M. TANIHARA, *J. R. Soc. Interface* **2** (2005) 373
22. A. OYANE, M. UCHIDA, Y. YOKOYAMA, C. CHOONG, J. TRIFFITT and A. ITO, *J. Biomed. Mater. Res. A* **75A** (2005) 138
23. C. G. PITT, T. A. MARKS and A. SCHINDLER, In: R. BAKER (ed). *Controlled release of bioactive materials*, (Academic Press: New York, 1980)
24. M. FINI, S. GIANNINI, R. GIARDINO, G. GIAVARESI, M. GRIMALDI, N. N. ALDINI, L. ORIENTI and M. ROCCA, *Inter. J. Artif. Organ* **18** (1995) 772
25. M. KELLOMAKI, H. NIIRANEN, K. PUUMANEN, N. ASHAMMAKHI, T. WARIS and P. TORMALA, *Biomaterials* **21** (2000) 2495
26. K. E. TANNER, R. N. DOWNES and W. BONFIELD, *Brit. Ceram. Trans.* **93** (1994) 104
27. S. B. CHO, K. NAKANISHI, T. KOKUBO, N. SOGA, C. OHTSUKI, T. NAKAMURA, T. KITSUGI and T. YAMAMURO, *J. Am. Ceram. Soc.* **78** (1995) 1769
28. H. M. KIM, F. MIYAJI, T. KOKUBO and T. NAKAMURA, *J. Biomed. Mater. Res.* **38** (1997) 121
29. D. T. CLARK, B. J. CROMARTY and A. DILKS, *J. Polm. Sci. Polm. Chem. Ed.* **16** (1978) 3173
30. A. Dilks, VanLaeken, *Physiological aspects of polymer surfaces*, edited by K. L. Mittal (Plenum: New York, 1983), p 749
31. T. HIROTSU, K. NAKAYAMA, T. TSUJISAKA, A. MAS and F. SCHUE, *Polym. Eng. Sci.* **42** (2002) 299
32. A. OYANE, M. UCHIDA, Y. ISHIHARA and A. ITO, *Key. Eng. Mater.* **284–286** (2005) 227
33. A. S. POSNER, *Physiol. Rev.* **49** (1969) 760
34. A. OYANE, K. ONUMA, T. KOKUBO and A. ITO, *J. Phys. Chem. B* **103** (1999) 8230
35. K. ONUMA and A. ITO, *Chem. Mater.* **10** (1998) 3346
36. J. C. ELLIOT, *Structure and chemistry of the apatites and other calcium phosphates*, (Elsevier Science BV: Amsterdam, 1994), pp. 1–61